



Electrical Engineering

**Experimental Investigations of Surface Break Down
Characteristics on Insulators in High Voltage Direct
Current Systems**

submitted as a RESEARCH REPORT FOR THE MARSHALL FOUNDATION

by

Robin Ramin BSc

25.September 2020

Project supervisors

Dr. Peter Zeller

Dr. Michael Steurer

Additional advisor

Dr. Gian Carlo Montanari

Acknowledgements

I want to thank the FSU staff for the great organization during the application process and when I had to return to Austria due to the pandemic. Special thanks to my additional advisor Gian Carlo Montanari for supporting me with his expertise in high voltage engineering and to Peter Cheetham for giving me advice in COMSOL.

Also thanks to the Marshall foundation, which made this project possible through funding.

Abstract

Designing and specifying DC spacers for transportation application is not as straightforward and well assessed as for sinusoidal AC. In particular, the electric field behavior in the presence of voltage transients, including energization and voltage polarity inversion, voltage harmonics, ripple, and temperature variation, has to be considered as unavoidable conditions in a dynamic and innovative electrical assets as those figuring out in electric ships and aircraft. This paper presents a COMSOL-based simulation of electric fields on DC spacer (bulk and surface) in dynamic conditions, highlighting the differences and common points with AC sinusoidal supply. The temperature in the model is adjustable to observe the effect of thermal gradients onto the spacer conductivity and field. The voltage value and waveform can be chosen freely and the operation can change between dynamic and stationary. It is known that during voltage transients the field is driven first by permittivity and tends slowly to the conductivity-driven field expected in steady state DC. The time to reach steady-state conditions can last hours, depending on dielectric properties and temperature. It has been also speculated that frequent voltage overshoots in DC systems can have an effect on the insulation lifetime. The change in field distribution due to transient voltages and thermal gradients in sinusoidal AC and DC is simulated and discussed. It is shown that voltage transients cause variation of internal and surface electric field that reaches steady state DC conditions in times that are orders of magnitude longer than the voltage transient time, and that thermal gradients have an significant impact on the field distribution, especially the bulk field. The difference in field distribution between sinusoidal AC and steady state DC operation is discussed for insulation components in hybrid systems. The potential impact of this dynamic behavior on spacer design looking at creepage and clearance specifications, is discussed and the effect of pollution is roughly mentioned.

Contents

Acknowledgements	II
Abstract	III
1 Introduction	1
2 Scientific question	3
3 Approach	4
4 Theory	6
4.1 Types of fields	7
4.1.1 Static & Stationary fields	8
4.1.2 Quasi-stationary fields	8
4.1.3 Non-stationary fields	9
4.2 Display of potential and electric field	10
4.3 Multilayer insulation arrangements	10
4.3.1 Orthogonal interface to field	11
4.3.2 Tangential interface to field	11
4.3.3 Interface inclined to the field	13
5 Simulation model	14
5.1 Material properties	15
5.2 Physics and studies	18
5.2.1 Electrostatics	18
5.2.2 Electric currents	19
5.2.3 Heat transfer in solids	19
6 Simulations	21
6.1 Stationary simulation at different temperatures & voltages	21
6.2 Variation of the surface layer thickness	23
6.3 DC & sinusoidal AC field distribution	24
6.4 Electric field distribution in AC and DC, with temperature gradient . . .	25
6.5 Electric field transition with & without thermal gradients	27
6.6 Influence of voltage transients on surface field distribution	30
6.7 Influence of contamination on surface field distribution	31
7 Summary/Conclusion	33
8 List of figures	35
9 List of tables	37

1 Introduction

Full and/or hybrid electrification of aircrafts and ships are going through a re-design of the electrical onboard system. The most obvious requisites for asset components are high power density, low weight, large power and energy dynamics, high efficiency and capability to withstand changes of missions. Especially in modern electrical assets, power electronics are replacing conventional voltage transformation, and, in addition, the concept of hybrid assets may force the same electrical insulation to operate under DC or power-electronics AC voltage, with high modulation and carrier frequency, repetitive voltage transients and harmonics [1–4]. However, the dramatic impact that hybrid voltage supply, corrupted AC sinusoidal waveforms or repetitive voltage transients can have on insulation reliability and on insulation system design is, perhaps, not yet understood properly [5, 6]. In addition to that, DC components may be subjected to frequent energizations, load variation, change of voltage polarity, voltage ripple superimposed to DC and temperature transients [5, 7]. These factors induce additional stresses that are often neglected when designing an electrical insulation systems. Considering that electrical insulation has a fundamental role for electrical asset safety and reliability, it could be speculated that what is beneficial to achieve the goals for increased specific power and efficiency may constitute as a threat for insulation components and asset reliability for voltage levels over 500-1000 V. As a consequence, and focusing on spacers and bushings, it is important to provide industry with specifications on creepage and clearance distance for the design of stand-off insulators for medium voltage DC (MVDC) ranges (1-30 kV). The clearance distance is the shortest distance in air between two conductive parts in a power system. It is dimensioned to withstand transient and impulse voltages, which are both fast breakdown mechanisms. Creepage distance is the shortest distance along the surface of a solid insulating material between two conductive parts in a power system. Higher voltage, frequency, operating temperature, repetitive voltage impulses, change of voltage waveform on the same insulation component, unpredictable modification of the electrical asset to fit to changes of mission: all of these will affect and generally worsen electrothermal, environmental and mechanical stresses, often in an unpredictable way, and potentially cause dramatic life and reliability reduction with respect to design specification of the insulation components [8–10]. A major difference is the electric field distribution, which is driven by insulating material conductivity in DC and by permittivity in AC, with a mix of both during each voltage transient as, e.g., energization, voltage polarity inversion, ripple, repetitive impulses. In the absence of defects which can alter the electric field, like gas-filled cavities, environmental issues (humidity, contamination) and temperature gradient, there is no change in field profile between AC and DC. However, the large dependence of conductivity on temperature, field and environmental factors can lead to significantly different electric field distribution in real operating conditions (both in the insulation bulk and on the surface). This is much less important in AC, because the permittivity variation due to temperature and environ-

mental factors is much lower than for electrical conductivity. A counter-action to these issues would be a redundant and conservative insulation system design, but this is not an option whether power density and weight are an issue. Therefore, the proper answer is to investigate the new types of stresses and associated ageing mechanisms, model life and put in place effective diagnostic tools that can allow Condition-Base Maintenance (CBM).

This report focuses on DC components whose design is not obvious, that is, insulating spacers. While design of spacers is well assessed and standardized for sinusoidal AC, there is not enough fundamental knowledge present to achieve the same for DC supply. It is therefore mandatory to study a DC insulation system under dynamic voltage supply. Another consideration that needs to be kept in mind is that while design of insulation fed by sinusoidal AC voltage has many decades of practice and feedback from operation, the same does not hold for DC, with the consequence that DC electrical insulation is often designed in conservative way, that is, low fields and temperatures. This cannot fit to the trend in industrial or transportation electrification assets. Electrical stress can be, as mentioned above, significantly different from sinusoidal AC, and it depends on temperature, thus load cycles and environment. Considering all the problems and uncertainty above, a finite-element simulation model has been developed to describe the behaviour of electric field in the bulk and on the surface of a DC insulation. While the model focuses on spacers, it can be extended to other type of insulation systems where surface properties play an important role, such as bushings. Section 2 describes the scientific question, which is answered in this report, followed by the the description on how the simulation model was created and verified (Section 3). Section 4 focuses on the fundamental theory of electric field in AC and DC. Then the foundation of the simulation setup and model is explained in Section 5 with its governing equations. Section 6 focuses on examples of simulations done from adjusting the surface layer thickness to DC and sinusoidal AC fields in isothermal environment as well as with thermal gradient. The effect of voltage transient and overshoots on the field is highlighted. As last simulations with surface contamination are briefly introduced as a guide for future work. In the conclusion, Section 7, the findings are commented, the current status of the model is described and future outlooks and ideas are mentioned.

2 Scientific question

The goal of this report is to design a finite element analysis model, which shall bring more insight on field behavior for thermal gradients, voltage transients and contamination in medium voltage DC systems. Furthermore, it shall be used to observe the field transition from permittivity-dependent to conductivity-dependent. The model is constructed in COMSOL and requires the electro- and thermodynamic physics. A spacer insulator between two electrodes has to be simulated for DC and AC voltage waveforms. The simulation model is required to compute stationary and time-dependent operations. The spacer must be separated into a bulk and a surface section. These two sections must have different conductivities and are a function of field and temperature. The model shall be used as a base to ease the way for surface breakdown forecasts and provide more efficient design tools for medium and high voltage spacers. Additionally, it shall be able to be upgraded and adapted to infer not only MVDC components of shipboard power systems, but in general MVDC assets and grid apparatus, The model shall also able to be a starting basis for partial discharge (PD) investigation.

3 Approach

The approach to get a functional and useful simulation model is summarized in the list below. First the dimensions of the stand-off insulator and the electrodes were gathered to create a 3D CAD geometry, which then was used as reference for the COMSOL model. Then the material properties of the objects used in the simulation were measured and researched. The application setup, busbar system, were imported into COMSOL. Next, the electrical and thermal aspects of the stand-off insulator setup had to be added to the model. Therefore, the physical models "electric currents" and "heat transfer in solids" were applied and adjusted. Additional physics to interlink the physics together were added. Then the insulator surface properties, conductivity, were modelled as a function of a temperature and the electric field. After that, the stationary simulation was upgraded to a time-dependent one to allow observing changes in the field over time. After evaluating and verifying the results of the model, different voltage operations were simulated. As first operation, different voltage transients were added to represent switching and energizing processes in the DC system. Then DC biased ripples, which should represent the remains of sinusoidal AC signals after rectification or diffusion from power electronics, were added. A test setup was built to measure surface charge, but at the time of this report we were not able to get exhaustive experimental data to be used to support the model. However, first observations were encouraging. Also, charging current measurements on specimens made of the same material of the simulated spacer are being carried out to support the values considered for conductivity and its dependence on temperature and field.

The goals of this project are to:

1. Create 3D models of the used objects [Completed]
2. Gather material properties for the objects [Completed]
3. Create the physical environment for model in COMSOL [Completed]
4. Adjust/Configure "electric currents" physic in COMSOL [Completed]
5. Adjust/Configure "heat transfer in solids" physic in COMSOL [Completed]
6. Configure additional physics in COMSOL (if necessary) [Completed]
7. Implement the surface conductivity dependence with temperature into COMSOL [Completed]
8. Change from stationary to 'time-dependent' study: Simulate voltage ripples and transients [Completed]
9. Finish the simulation model [Completed]
10. Plan the measurement procedure [Completed]

11. Build the measurement setup [Completed]
12. Do the measurement [Open]
13. Compare simulation with measurement results [Open]

4 Theory

The following theory in this chapter was mostly summarized from Küchler [11]. In high voltage engineering, problems can vary from simple to complex, however, as complex as the problem might be, the problem can always be described by Maxwell's equations (Faraday's law, Ampere's law, Continuity equation), see Eq. 4.1-4.5. The field equation Eq. 4.1 & 4.2 describe the time-varying coupling between electric and magnetic quantities in terms of induction and magnetomotive force. The continuity equation Eq. 4.3 to 4.5 describe the continuity and sources of electric and magnetic field quantities.

Faraday's Law (Law of induction)

$$\oint_x E dx = -\frac{\delta}{\delta t} \iint_A B dA \quad (4.1)$$

Ampere's Law (Law of magnetomotive force)

$$\oint_x H dx = \iint_A J + \frac{\delta D}{\delta t} dA \quad (4.2)$$

Continuity Equation for magnetic flux density

$$\oiint_A B dA = 0 \quad (4.3)$$

Continuity Equation for displacement current density

$$\oiint_A D dA = Q \quad (4.4)$$

Continuity Equation for conduction & displacement current density

$$\oiint_A J + \frac{\delta D}{\delta t} dA = 0 \quad (4.5)$$

Where E is the electric field strength, B the magnetic flux density, x the path length, A the area, H the magnetic field strength, J the current density, D the dielectric displacement field and Q the electric charge. In addition to Maxwell's equation there are three material equations to describe the field quantities under the influence of different material properties (Eq. 4.6-4.8). The magnetic flux density is described by the magnetic field strength and the permeability μ of the material, see Eq. 4.6. The dielectric displacement field is related to the field generating charges and is proportional to the electric field strength, see Eq. 4.7. The permittivity ϵ describes the polarization of the material and depends on frequency and temperature. ϵ_0 is the permittivity of vacuum with 8.8542 pF/m and ϵ_r is the relative permittivity describing the material property. The relative permittivity is always bigger

than 1 because any available electric charge is polarized in the electric field and therefore it is higher than the permittivity in vacuum. The relative permittivity of air is usually assumed to be 1 because its value is negligibly higher than that of vacuum. On an ideal conductive electrode, the dielectric displacement field corresponds to the surface charge density σ_Q (Eq. 4.9). The last material equation (Eq. 4.8) describes the current density, which is proportional to the electric field strength and the electrical conductivity σ . Where the electrical conductivity describes the acceleration of mobile charge carriers due to an applied electric field. Mobile charge carriers are electrons and ions. In conductors the conductivity is governed by electrons and in dielectrics by ions. The relation in Eq. 4.8 is linear for solids, however, if the environmental properties (for example temperature) change, then the relation gets non-linear. The same applies to liquids and gases. The conductivity in air has no linear relation for high electric field strengths and if radiation is present. First saturation effects occur and with even higher electric field strengths the conduction increases rapidly due to additional production of free charge carriers due to impacts. The conductivity of material can be influenced by:

- Material properties (gaseous, liquid, solid)
- Impurities in the material (air bubbles, contamination, humidity, water content in oils)
- Mechanical stress (micro cracks)
- Temperature
- Electric field strengths
- Radiation
- Pressure

$$B = \mu_0 \mu_r H \tag{4.6}$$

$$D = \epsilon_0 \epsilon_r E \tag{4.7}$$

$$J = \sigma E \tag{4.8}$$

$$D = \sigma_Q \tag{4.9}$$

4.1 Types of fields

Considering the effect of time on a field, then three kinds can be distinguished. First static & stationary fields, also called steady-state fields, these fields are not time-variant. Second are quasi-static fields, which slowly change over time. Hence the electromagnetic coupling in these fields is weak and can be neglected. And third are non-stationary fields, which change fast over time and have a strong electromagnetic coupling.

4.1.1 Static & Stationary fields

In this fields no change occurs over time, hence all derivatives over time yield zero and no change in the electric field strength, magnetic field and current density. This also yields to no coupling between electric and magnetic quantities. Maxwell equations are changed accordingly to

$$Eq. 4.1 \rightarrow \oint_x E dx = 0 \rightarrow \sum_i V_i = 0 \quad (4.10)$$

$$Eq. 4.2 \rightarrow \oint_x H dx = \iint_A J dA = I \quad (4.11)$$

$$Eq. 4.5 \rightarrow \oiint_A J dA = 0 \rightarrow \sum_i I_i = 0 \quad (4.12)$$

The electric field is irrotational (conservative), hence it can be written as the sum of all voltages yields zero. The electric field can be determined by the gradient of the potential scalar field φ , see Eq. 4.13.

$$E = -grad\varphi \quad (4.13)$$

Propagation of electromagnetic waves is therefore not possible as well. They can only be apparent when fixed in time and location. In static fields energy transport is not possible, hence $J=0$ and the electric field strength only depends on the dielectric displacement field and therefore on the permittivity. This environment is only theoretically possible since it requires a perfect dielectric with zero conductivity, which is impossible to create in reality. In stationary fields, energy transport is possible and hence constant currents can flow. The permittivity has no significant effect in stationary fields, that yields an electric field strength dependent on the conductivity, called resistive field. Constant direct current applications are always stationary fields.

4.1.2 Quasi-stationary fields

In quasi-stationary fields the field dependent quantities change slowly over time, however the coupling between electric and magnetic field is weak, such that the induced electric curl field from the magnetic field caused by the displacement current can be neglected. The displacement current however, cannot be neglected. Quasi-stationary fields can be distinguished into inductive and capacitive fields. Inductive fields are found in materials with high conductivity, while capacitive fields are found in materials with low conductivity. It is distinguished between the two by using Eq. 4.14. If the condition in this equation is true, then the dielectric displacement field can be neglected. In case the condition is false, nothing can be neglected.

$$\frac{\delta D}{\delta t} = \epsilon \frac{\delta E}{\delta t} \ll J = \sigma E \quad (4.14)$$

In inductive fields even low electric field strengths cause a high conduction current due to a high conductivity value. Hence there is a coupling between electric and magnetic field.

The electric field is not conservative any more and is described by Eq. 4.1, 4.11, 4.3, 4.4, 4.12, 4.6 and 4.8.

Capacitive fields describe the field in dielectric materials where the permittivity is much higher than the conductivity. Only Faraday's law can be adapted in this situation as shown in Eq. 4.10. The electric field is irrotational, therefore Eq. 4.13 is valid. Capacitive fields can describe most cases of power frequency voltage (AC), Switching Impulse (SI) voltage and Lightning Impulse (LI) voltage, which are the origin for the most important voltage stresses on insulation material.

In quasi-stationary fields all changes of the field must happen nearly synchronously, then travelling wave processes can be neglected since they have to be considered for fast changing fields. In case of steady-state operation with a predominant current, the capacitive field transitions into a resistive field. To distinguish between a capacitive and a resistive field, the dielectric time constant τ_d for transient behaviour is used. The dielectric time constant is found from the equivalent RC-network model. The dielectric time constant for a homogeneous capacitor arrangement is given by [12, 13]:

$$\tau_d = \epsilon_0 \epsilon_{rb} / [\sigma_b(T(x, y, t), E(x, y, t))] \quad (4.15)$$

If the field change is much faster than the dielectric time constant, then a capacitive field can be assumed.

Examples for changes are

- AC quarter-period →

$$T/4 \ll \tau_d \quad (4.16)$$

- Voltage rise time →

$$T_{rise} \ll \tau_d \quad (4.17)$$

In case the field change is much slower than the time constant one considers a resistive field. When the change in voltage comes to an halt, the capacitive field changes with respect to the dielectric time constant into a resistive field. This change takes approximately $5\tau_d$ and can take several hours.

4.1.3 Non-stationary fields

Non-stationary fields change rapidly with time and have strong coupling between electric and magnetic field. Electromagnetic wave propagation, propagation time effects and spatial dimensions must be considered. There is no simplification of Maxwell's equations possible.

4.2 Display of potential and electric field

Graphical analysis of electric fields gives a lot of information like non-uniformity of the field, stress points and potential as well as field distribution. First, there are equipotential lines, these are contours where the potential stays the same, they are displayed in rainbow colours in 4.1. They are always orthogonal to electric field lines (black). Charges on equipotential lines can move without any force or energy. The potential difference between the lines is constant (Eq. 4.18).

$$\Delta\varphi = const. \quad (4.18)$$

Second, electric field lines, these lines are distanced with a constant charge on the electrode (Eq. 4.19). Dense electric field lines indicate a high charge distribution and therefore a high electric field strength.

$$\Delta Q = const. \quad (4.19)$$

An enclosed field of equipotential lines and electric field lines has a constant capacitance.

$$\Delta C = \frac{\Delta Q}{\Delta\varphi} \quad (4.20)$$

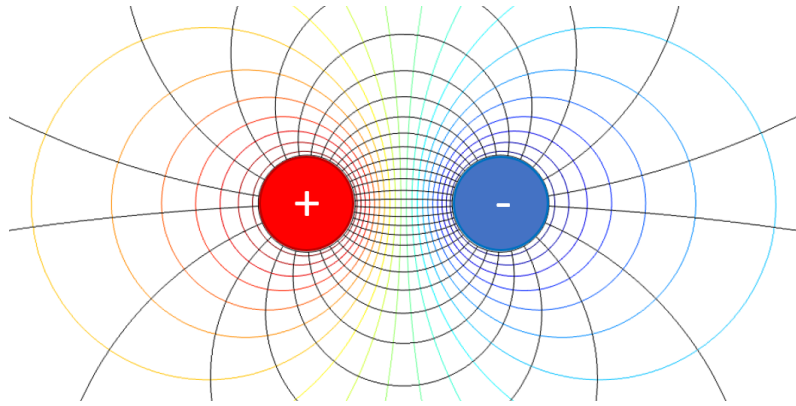


Figure 4.1: Display of an electric field between two opposite charges

4.3 Multilayer insulation arrangements

In electric systems the insulation does sometimes consists of different materials be it by choice or due to constrictions. The electric field can be affected by the change of material depending on the material quantities and the direction, the field lines enter the new material. Considering a boundary as in Fig. 4.2, one can integrate the electric field strength on the small closed path P1-P2-P3-P4-P1 as following

$$Eq. 4.10 \rightarrow \oint_s E ds = sE_{1T} + (-sE_{2T}) = 0 \rightarrow$$

$$E_{1T} = E_{2T} \quad (4.21)$$

Therefore, the tangential field component is not affected by the transition into the other material. In resistive fields it follows $J_{1N} = J_{2N}$ and in capacitive fields $D_{1N} = D_{2N}$.

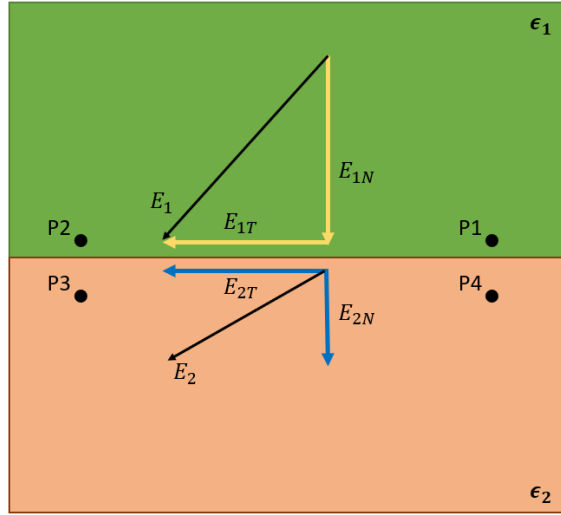


Figure 4.2: Electric field strength vectors at material interface

4.3.1 Orthogonal interface to field

Considering the case of an arrangement as in Fig. 4.3 with two materials which have different field material properties and the interface orthogonal to the field. The normal quantity of the material dielectric displacement density has the same magnitude as the field quantity ($D_1 = D_2$). Respectively the current density ($J_1 = J_2$), if the field is a resistive field. The electric field strength relation between both materials for a dielectric displacement field is

$$E_1 \epsilon_1 = E_2 \epsilon_2 \quad (4.22)$$

The material with the higher permittivity is stressed less by the electric field strength. The sum of both electric field strengths yields the total field strength. No refraction of the field is observed at interfaces orthogonal to the electric field, hence the tangential field component is zero.

4.3.2 Tangential interface to field

In case of an arrangement as in Fig. 4.4 the interface is tangential to the electric field. This yields that the electric field strengths magnitude in both materials and the total electric field strength magnitude are equal.

$$E_1 = E_2 = E \quad (4.23)$$

Hence the dielectric displacement densities are different Eq. 4.24, more charge accumulates on the electrode where the material with the higher permittivity is contacting. In a resistive

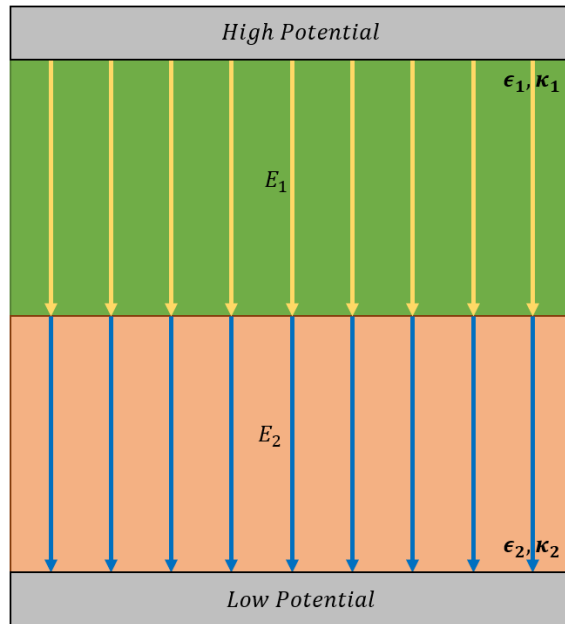


Figure 4.3: Orthogonal interface to the el. field in a parallel-plate capacitor

field the current density in one material would be higher depending on the electrical conductivity.

$$\frac{D_1}{\epsilon_1} = \frac{D_2}{\epsilon_2} \tag{4.24}$$

It seems that this kind of interface has good insulation properties, however in reality it is observed to have lower electric breakdown fields. This is caused by different surface properties between surface and bulk, voids in the interface, micro roughness, contamination on the surface.

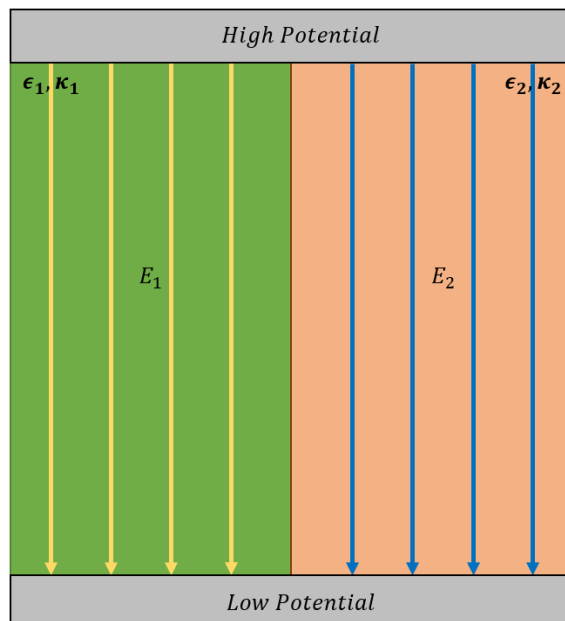


Figure 4.4: Tangential interface to the el. field in a parallel-plate capacitor

4.3.3 Interface inclined to the field

Inclined means the interface has an angle between 0° and 90° . From Eq. 4.21 it is concluded, that the tangential field component stays constant at the interface of two materials. Hence only the normal field component is changing, this was observed in subsection 4.3.1 and is represented as

$$E_{1N}\epsilon_1 = E_{2N}\epsilon_2$$

The angle between the normal on the interface and the electric field vector can now be calculated with the inverse tangent of the quotient from the tangential and normal component to the interface as

$$\tan(\alpha) = \frac{E_T}{E_N} \quad (4.25)$$

Hence one can write the relation between both materials as

$$\frac{\tan(\alpha_1)}{\tan(\alpha_2)} = \frac{\epsilon_1}{\epsilon_2} \quad (4.26)$$

This is called the refraction law. The electric field strength in the material with the higher permittivity is refracted towards the interface and the material with the lower permittivity towards the surface normal. The same can be applied to the conductivity in a resistive field.

5 Simulation model

For better analysis of the field behaviour components in medium voltage DC systems, a simulation in COMSOL Multiphysics was created. For the start, the simulated setup was held simple to have shorter computation times of the model and to get a better understanding on the effects happening in the simulated setup. The simulated setup consists of a cylindrical stand-off insulator (spacer) between two electrodes, as shown in Fig. 5.1. The electrodes on top and bottom in grey are made of aluminium, while the insulator is made of glass-mat reinforced polyester (GPO-3). The edges of the electrodes are rounded to avoid large field gradients as those occurring in case of squared contours. The spacer form and size are inspired by real products on the market, which have nominal voltage of around 3.2 kV. The setup is surrounded by air at 20 °C and a pressure of 1 atm. The top electrode has an electric potential of 10 kV and the bottom electrode is grounded (0 V). The reason for using a far higher electrode voltage than the nominal voltage, lies in the dimensions. Insulators are build to withstand far more than the nominal voltage, therefore they are designed to have a low electric field when operated under nominal voltage. By using a higher voltage, the field distribution will be more distinctive. The geometry is 2D axisymmetric hence it takes less afford to simulate the geometry, this is shown in Fig 5.2.

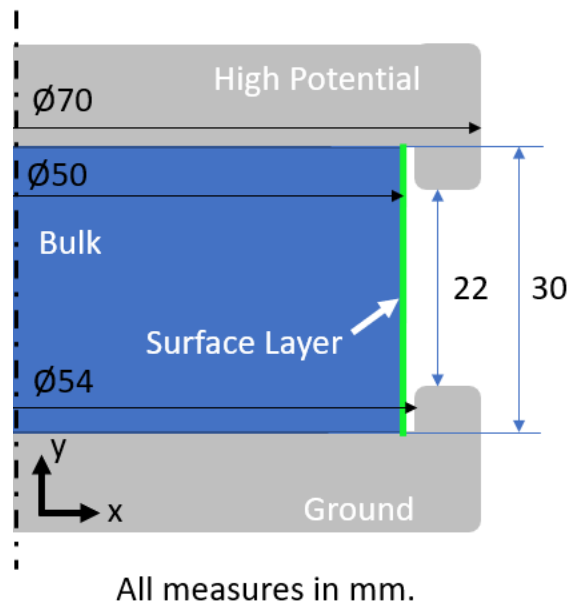


Figure 5.1: Axis-symmetric drawing of the spacer used for COMSOL simulations with a surface layer of 0.1 mm.

The modelled insulator is split into two parts, bulk and surface layer. The latter is used to simulate the different surface conductivity properties compared to the bulk conductivity. In real insulators the surface layer is caused by a different microstructure and can have conductivity values with orders of magnitude higher than the bulk [14, 15]. The surface layer is assumed to have a thickness of 100 μm . A thinner layer does not change the

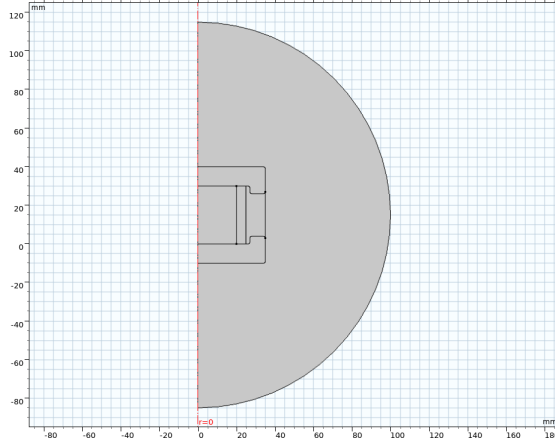


Figure 5.2: 2D axisymmetric model of the setup in COMSOL

simulation results greatly, see Fig. 6.4.

5.1 Material properties

The setup is placed in a default environment with an ambient pressure of 1 atm and an ambient temperature of 20 °C. The material parameter for the object in the setup are summarized in Table 5.1. The parameter for air are pre-set by COMSOL and were not altered, except the electrical conductivity for air, which was set between the values mentioned in [11, 16]. The temperature conductivity, heat capacity and density for air are modelled as described in Eq. 5.1-5.3. Where λ_{Air} is the thermal conductivity dependent on temperature, C_{Air} the specific heat capacity dependent on the temperature and ρ_{Air} the density dependent on the pressure and the temperature. The electrode material, aluminium, was taken as well from the COMSOL library.

$$\lambda_{Air}(T) = -0.00227 + 1.15480 \cdot 10^{-4}T - 7.90252 \cdot 10^{-8}T^2 + 4.1170 \cdot 10^{-11}T^3 - 7.43864 \cdot 10^{-15}T^4 \quad (5.1)$$

$$C_{Air}(T) = 1047 - 0.37258T + 9.45304 \cdot 10^{-4}T^2 - 6.02409 \cdot 10^{-7}T^3 + 1.28589 \cdot 10^{-10}T^4 \quad (5.2)$$

$$\rho_{Air}(P, T) = \frac{0.02897P}{8.3144T} \quad (5.3)$$

The density, thermal conductivity and relative permittivity for the spacer were taken from a GPO-3 specsheet¹. The electrical conductivity and thermal conductivity are taken from [13]. The surface conductivity is always lower than the bulk conductivity, due to the microstructure difference. The electrical conductivity in the bulk and the surface layer was modified to depend on the electric field and temperature difference. The relation is described by the Arrhenius equation, see Eq. 5.4.

¹<http://www.polyplycomposites.com/sheet.pdf>

Table 5.1: Material parameter of the insulator material and air

Material parameter	Insulator Bulk	Insulator Surface	Air
Electrical conductivity σ_0 [S/m]	8e-17	8e-16	8e-15
Temperature dependent coefficient α [1/K]	0.1	0.1	-
Electric field dependent coefficient β [mm/kV]	3.4e-2	3.4e-2	-
Reference electric field E_0 [V/m]	0	0	-
Reference temperature T_0 [°C]	5	5	-
Relative permittivity ϵ_r	4.8	4.8	1
Thermal conductivity λ [W/(mK)]	0.274	0.274	$\lambda_{Air}(T)$
Density ρ [kg/m ³]	1800	1800	$\rho_{Air}(P, T)$
Heat capacity C_p [J/(kgK)]	1900	1900	$C_{Air}(T)$

$$\sigma = \sigma_0 e^{-E_A/kT} \quad (5.4)$$

σ_0 is the reference conductivity, E_A is the activation energy, k the Boltzmann constant and T is the absolute temperature. The activation energy is gained by the difference of the mobility edge energy and the fermi energy. This version of the Arrhenius equation is difficult to apply for real materials, since they usually have non-uniform lattice and the measurement afford to find the activation energy is too high. Hence there are more practical versions of it, which are gathered through empirical data. A popular simplified version is shown in Eq. 5.5.

$$\sigma(E, T) = \sigma_0 e^{\alpha(T(x,y,z,t)-T_0)+\beta|E(x,y,z,t)-E_0|} \quad (5.5)$$

σ_0 is the conductivity at reference temperature T_0 , α is the temperature coefficient, β is the field dependency coefficient and E_0 is the reference electric field strength. α and β are the empirical quantities. With this equation, the conductivity can increase 4 to 5 orders of magnitude from ambient to operation temperature.[11, 17]

In the paper from Occhini [17] an another version is described, see Eq.5.6. Where σ_0 is the reference conductivity and a , which is an empiric constant. This version is closer to the real behaviour of the conductivity, however, there is again a higher afford in measuring the quantity a , which makes it unpractical.

$$\sigma(E, T) = \sigma_0 e^{-\frac{a}{T(x,y,z,t)}+\beta|E(x,y,z,t)|} \quad (5.6)$$

Therefore, Eq. 5.5 is used. Since α and β are not known for GPO-3 yet, it was assumed

Table 5.2: Constant values used for finding the right reference temperature

Material parameter	Value for Eq. 5.5	Value for Eq. 5.6
a [K]	-	11e3
α [1/K]	0.105	-
β [mm/kV]	0.034	-
σ_0 [S/m]	5.7e-17	4.3

that GPO-3 has the same or at least similar properties as the oil-impregnated paper in Occhini's paper [17], see Table 5.1. Using different material values for the simulation results in yields wrong field strength values, but it gives a similar distribution and this is enough to further upgrade the current simulation. Since the reference temperature used is not stated in Occhini's paper, Eq. 5.5 was fit to Eq. 5.6 for the range 0 to 100 °C to figure out the used reference temperature. For the comparison, the electric field strength was set to 0 V/m because it influences the conductivity equally in both equations. E_0 is set to 0 V/m as well. The values for the constants are shown in Table 5.2. The fit, see Fig. 5.3, showed that the reference temperature is likely to be at 5 °C. Therefore, 5 °C is used as reference temperature for Eq. 5.5 in the simulation. It is noteworthy, that Eq. 5.5 with the used constants should only be applied in the range of 20 to 90 °C since the deviation between simplified and accurate Arrhenius equation will strongly increase outside of this range.

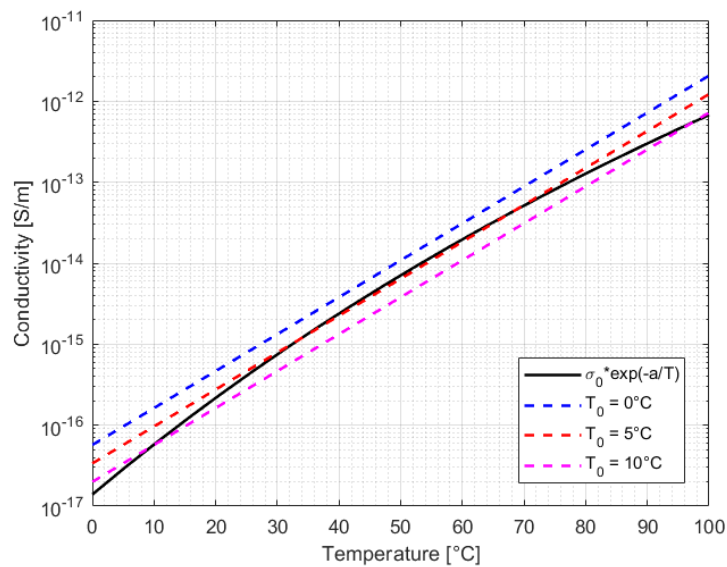


Figure 5.3: Comparison of Eq. 5.6 (full line) and Eq. 5.5 (dotted lines) for different reference temperatures T_0 . The field is 0 kV/mm.

5.2 Physics and studies

To achieve reasonable simulation results, the correct physics as well as studies need to be added in COMSOL. The used physics „electrostatics“, “electric currents” and “heat transfer in solids” were used and are explained in the following subsections. Electromagnetic coupling was neglected because the coupling in the setup is very weak. To combine the heat generated through current and the heat transfer in the model, the multiphysic “electromagnetic heating” was added. Since the spacer setup carries just small currents, “electromagnetic heating” wouldn’t be necessary. However, if the setup will be changed in the future, the basic physics don’t need to be changed. As studies the “stationary”, “frequency-domain” and “time-dependent ” study were used to get results for AC and DC waveforms in stationary and time-variant settings. As the name “stationary” already suggests, the study calculates the field distribution after infinite of time for transients and DC voltages. Later in this simulation model the “stationary” study was used to get the steady-state DC field distribution and to get initial results for simulations over time. The “frequency-domain” is used to calculate field distributions for steady alternating waveforms. The “time-dependent” study is used whenever a time-variant event happens like voltage transients, ripple, energizing of the setup,

5.2.1 Electrostatics

From the governing equations in COMSOL it is clear that the resulting field from the “electrostatic” physic is a static field, hence no current is calculated and therefore only the permittivity is used for calculations, as described in subsection 4.1.1. Hence the results for the “stationary” and “frequency-domain” study are identical and are shown in Fig. 5.4. The result is indeed a capacitive field because the field lines at the interface of spacer and air show a refraction angle, which breaks the field line in the air domain towards the normal of the interface. From Eq. 4.26 it is associated that the electric field component in the spacer is greater than the one in air. This proves, that the field is dependent on the permittivity, hence $\epsilon_{spacer} > \epsilon_{air}$. The “electrostatic” physic was used in previous versions of the simulation to verify the field behaviour in the early stage of the model, but was then replaced by the “electric currents” physic.

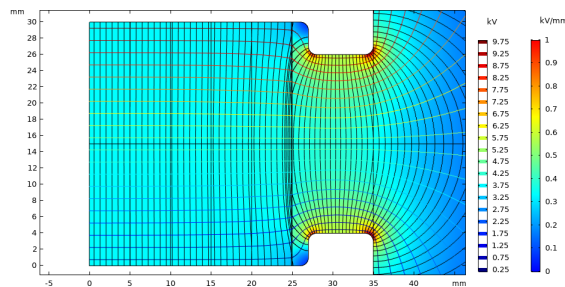


Figure 5.4: Electric field norm simulated with the “electrostatics“ physic for an electrode voltage of 10 kV DC.

5.2.2 Electric currents

In “electric currents” a quasi-stationary field is simulated, as it was described in subsection 4.1.2. Therefore it was necessary to figure out when Comsol is calculating a capacitive field and when a resistive field. By using different studies it was proven that Comsol simulates a resistive field distribution in the “stationary” study, see Fig. 5.5a, while simulating a capacitive field distribution for the “frequency-domain” study, see Fig. 5.5b. The change in refraction angle indicates that the field is calculated with the conductivity for the “stationary” study and with the permittivity for the “frequency-domain” study. Another indicator is, that Fig. 5.4 and Fig. 5.5b are identical, hence the field must be capacitive.

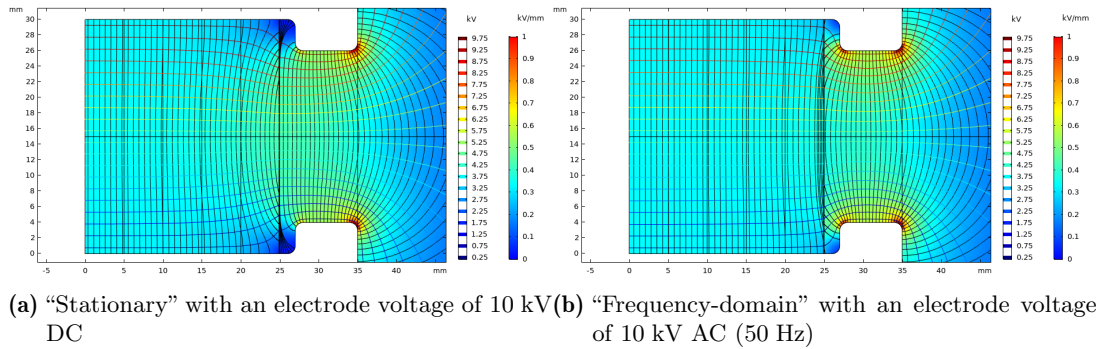


Figure 5.5: Electric field norm simulated with the “electric currents“ physic

5.2.3 Heat transfer in solids

This physic is used to simulate temperature and temperature gradients in the simulated domain. The physic is governed by Eq. 5.7 & 5.8. Where ρ is the density, C_p the specific heat capacity, u is the velocity vector, q is the conductive heat flux, Q is the heat source, Q_{ted} is the thermoelastic damping and k is the thermal conductivity. The outside boundary and the lower electrode are fixed to 20 °C, as reported in Fig. 5.6 (highlighted in blue). The top electrode temperature is changed between 0 and 100 °C, depending on the simulation setup. Since all simulations were done at a thermal equilibrium, the fixed boundary condition on the outside didn’t affect the simulation results. Hence when heat sources or different temperatures were present in the simulation domain, a stationary study for the temperature distribution was done before the time-variant simulation.

$$\rho C_p \frac{\delta T}{\delta t} + \rho C_p u \cdot \nabla T + \nabla \cdot q = Q + Q_{ted} \quad (5.7)$$

$$q = -k \nabla T \quad (5.8)$$

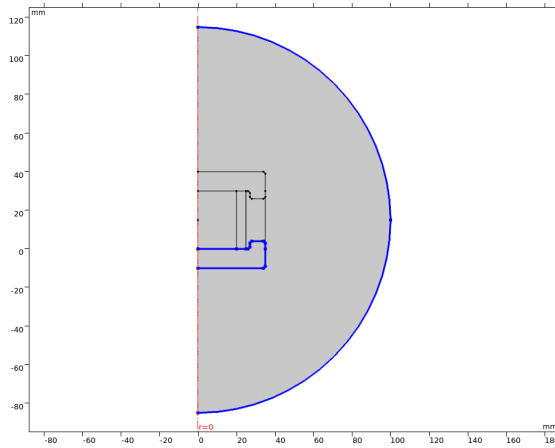


Figure 5.6: Boundaries fixed to 20 °C.

6 Simulations

First, the model was tested for its fundamental boundaries and rules after all necessary physics, material properties, studies, geometries were set. One part of it was to figure out if the right equations for calculating the field were used for different applied voltages (this was already covered in subsection 5.2.2). Then the temperature and voltage was altered in a “stationary” study to test, if the “heat transfer in solids” physic and the conductivity equation (Eq 5.5) were working properly. After that, the effect of different surface layers on the field distribution was observed. After these tests, which are dealt with in the following sections, the simulation was proven to work as intended. With that knowledge further simulations were done to get more insight into the field behaviour under DC compared to sinusoidal AC with and without thermal gradients. The transition time it takes to change between capacitive to resistive field is dealt with as well as the field behavior for different voltage transients. In the end, the topic surface contamination is roughly discussed.

In the rest of the report, the field is distinguished between the axial field, which is the the field component pointing into the Y-direction according to the coordination system presented in Fig. 5.1, the radial field, which is the the field component pointing into the X-direction according to the coordination system presented in Fig. 5.1, and the electric field norm, which is the norm of both, axial and radial, components.

6.1 Stationary simulation at different temperatures & voltages

Two different approaches were done to see the effect of the electric field strength and the temperature on the electrical conductivity and to verify the “heat transfer in solids” physic is working properly. Both approaches were done in the “electric current” physic and with the “stationary” study. First, the temperature was set constant to 20 °C in the whole domain and the voltage on the top electrode was changed from 20 to 60 and 100 kV. For all scenarios, the electric field and the electrical conductivity were observed, see Fig. 6.1. The conductivity in the insulator has the same pattern as the electric field and increases with higher voltages, which is due to Eq. 5.5. By taking some of the electric field values and calculating the conductivity from it via Eq. 5.5, it was possible to get close the same results as depicted in Fig. 6.1b, 6.1d & 6.1f. Hence it is concluded that the electric field dependency is working accurately.

After that the temperature of the top electrode was changed from 0 to 100 °C, while the bottom electrode was kept at 20 °C. The voltage on the top electrode was set to 0 V. The temperature and conductivity distribution were observed, see Fig 6.2. The conductivity distribution is strongly non-linear for thermal gradients (Fig. 6.2b & 6.2f) and in the case of isothermal conditions (Fig. 6.2d) the conductivity is uniform and the value is correct as

well. Hence the temperature dependency of the conductivity is working properly as well. The temperature distribution over the setup looks reasonable. Since all simulations are carried out after a thermal equilibrium has been established, this is sufficient enough to verify the correctness of the thermal simulation part.

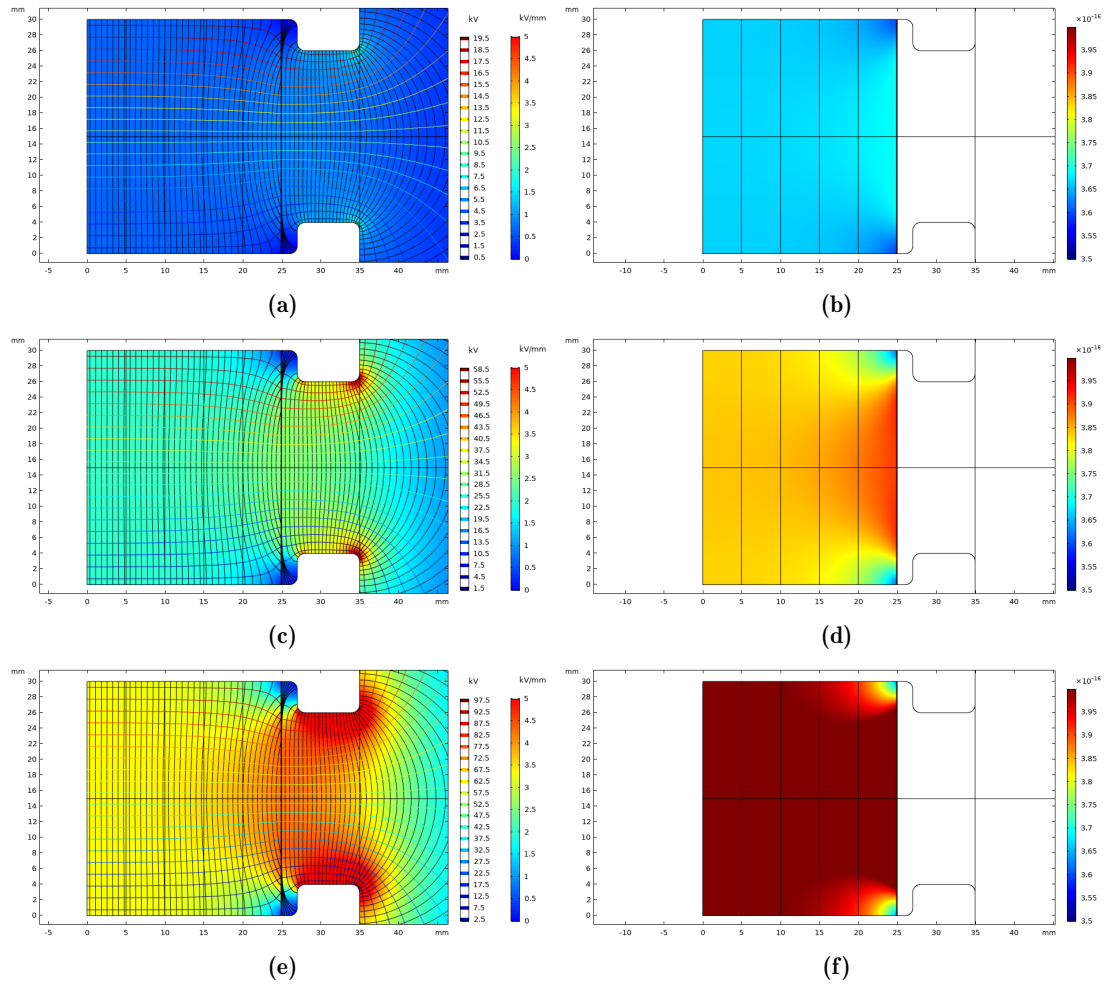


Figure 6.1: Changing voltage with isothermal condition (20 °C). Electric field norm (left) and conductivity in the insulator (right). 20 kV (6.1a & 6.1b), 60 kV (6.1c & 6.1d), 100 kV (6.1e & 6.1f)

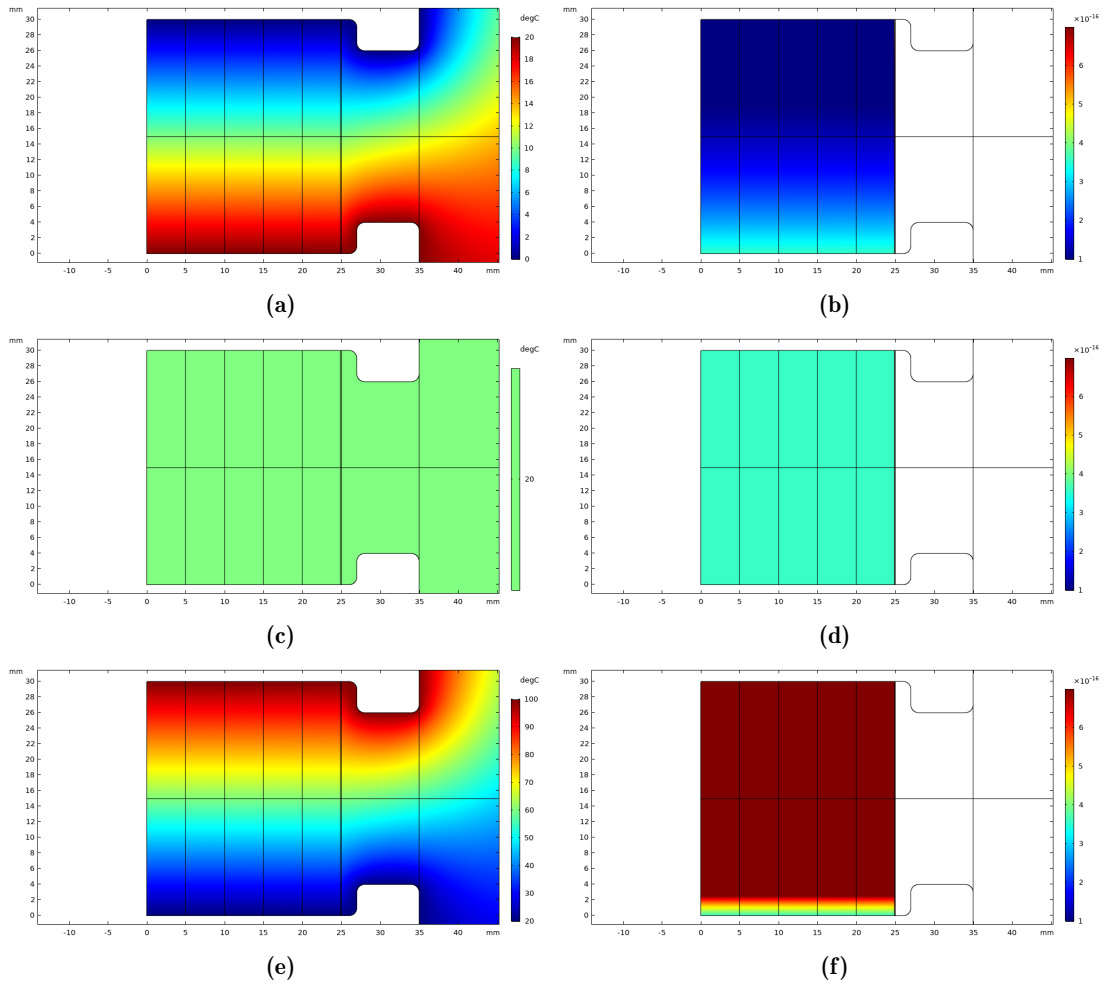


Figure 6.2: Constant voltage (0 V) with different temperatures. Temperature (left) and conductivity in the insulator (right). Temperature of the top electrode is 0 °C (6.2a & 6.2b), 20 °C (6.2c & 6.2d), 100 °C (6.2e & 6.2f)

6.2 Variation of the surface layer thickness

Simulations were carried out to find out, if the surface layer thickness has an significant impact on the field distribution on the surface. Three different surface layer thicknesses (0.1 mm, 0.01 mm, 1 μm) were simulated with a sufficient dense mesh, see Fig. 6.3. The field distribution for each thickness is reported in Fig. 6.4. It shows the axial field component (E_y) and the radial field component (E_x) along the surface. From the results it was concluded, that a thinner surface layer does not cause a significant field change, hence a surface layer thickness of 0.1 mm was used for all simulations because it allowed shorter computation times, since the mesh in the surface layer could be made more coarse.

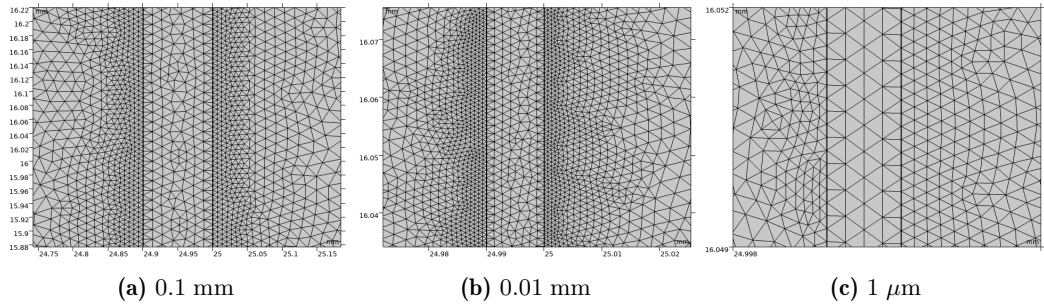


Figure 6.3: Triangular mesh in the surface layer and surrounding for different surface layer thicknesses. Units in mm.

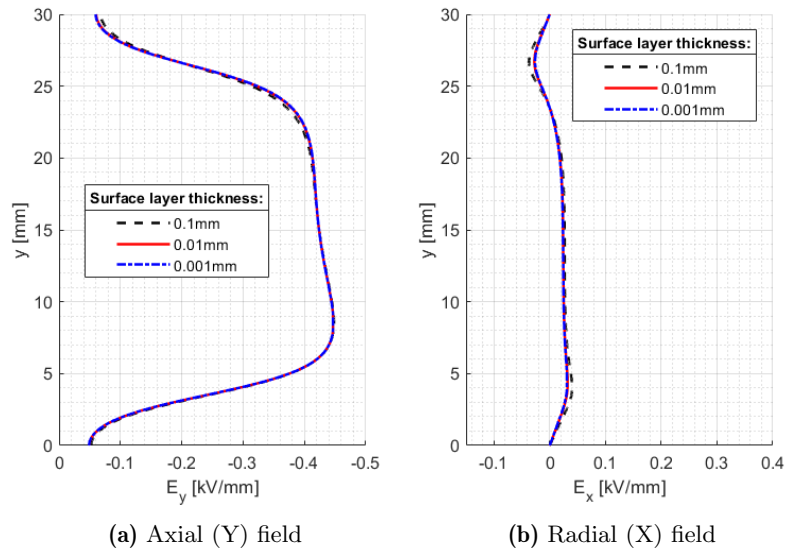


Figure 6.4: Steady-state DC field distribution along the surface for different surface layer thicknesses with a thermal gradient of 20 °C between the electrodes. The y-axis corresponds to the Y-direction of Fig. 5.1.

6.3 DC & sinusoidal AC field distribution

Figure 6.5a and 6.5b show an example of a steady-state DC simulation, compared with sinusoidal AC power supply, for the spacer. As expected, while AC and DC bulk fields almost coincide, the surface fields are noticeably different also in isothermal conditions. The reason for that is the interfaces between bulk, surface insulation layer and air, where different permittivity and conductivity values are involved. As a consequence, a higher axial field component E_y in steady-state DC is observed than in AC (increase by approx. 20 %), while the opposite occurs for the radial field component E_x (decrease by approx. 85 %). The surface field is kept low in the areas 0-5 mm and 25-30 mm due to the electrode geometry, yielding a higher field in the remaining area due to Eq. 4.13. In the bulk the conductivity is taken as uniform and, therefore, the field distribution is quite uniform as well. Hence the radial field component in the bulk is zero. Quantification of the difference between AC and steady-state DC field in the insulation (focusing mostly on the bulk),

and the contribution of a temperature gradient, as expected in service, are shown and discussed in the next Section.

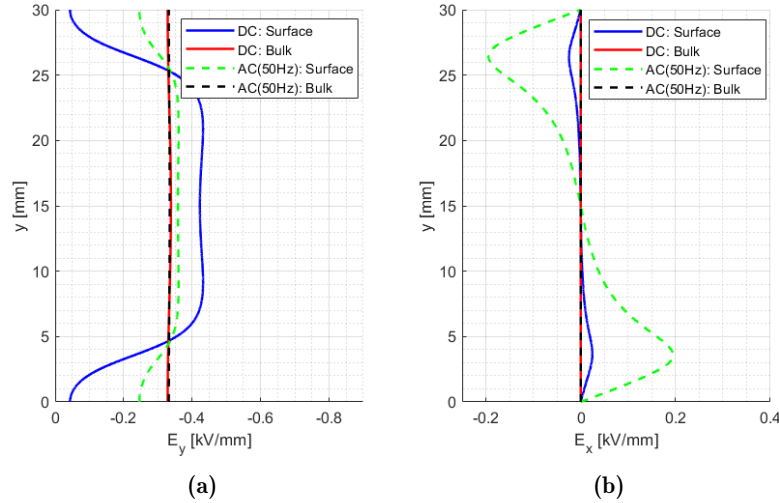


Figure 6.5: Axial steady-state DC [-] and sinusoidal AC (50 Hz) [-] field distribution for the surface and the bulk, 6.5a. Radial steady-state DC [-] and sinusoidal AC (50 Hz) [-] field distribution for the surface and the bulk, 6.5b. Simulated for isothermal conditions at 20 °C and 10 kV electrode voltage. The y-axis corresponds to the Y-direction of Fig. 5.1.

6.4 Electric field distribution in AC and DC, with temperature gradient

The electric field profiles along the Y-axis, for the bulk and the surface layer, are reported in Figs. 6.6a & 6.6b, referring to sinusoidal AC and steady-state DC, a temperature gradient of 20 °C. Larger temperature gradient, i.e. 40 °C, is considered in Fig. 6.7. Figure 6.6 shows that the curves for sinusoidal AC are identical to those reported in Fig. 6.10, since the field is ruled by the permittivity which does not depend onto the temperature. On the contrary, the steady-state DC profiles with thermal gradient differ significantly from the profile without temperature gradient because the field is governed by the conductivity and the conductivity depends noticeably on temperature, Eq. 5.5 and Table 5.1 (α). Considering the location, the steady-state field distribution on the surface is not as far from the isothermal field (2 % increase in max. axial field), while the field distribution in the bulk changes considerably from isothermal to thermal gradient conditions (94 % increase in max. axial field). The increase in axial field takes place in the lower temperature area, due to an increase in conductivity. On the surface the radial field is slightly increased as well due to the thermal gradient. The difference in the bulk becomes even more evident for the 40 °C gradient. Here the top electrode has a temperature of 60 °C.

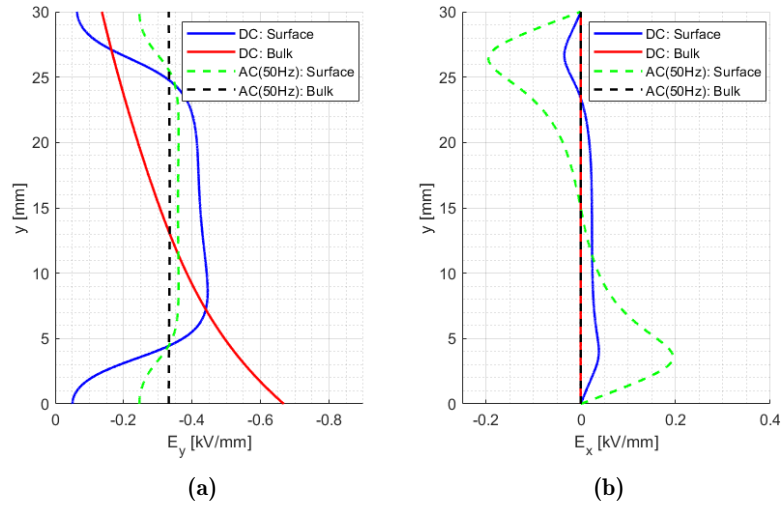


Figure 6.6: Axial steady-state DC [-] and sinusoidal AC (50 Hz) [-] field distribution for the surface and the bulk, 6.6a. Radial steady-state DC [-] and sinusoidal AC (50 Hz) [-] field distribution for the surface and the bulk, 6.6b. Temperature gradient of 20 °C, nominal voltage 10 kV. The y-axis corresponds to the Y-direction of Fig. 5.1.

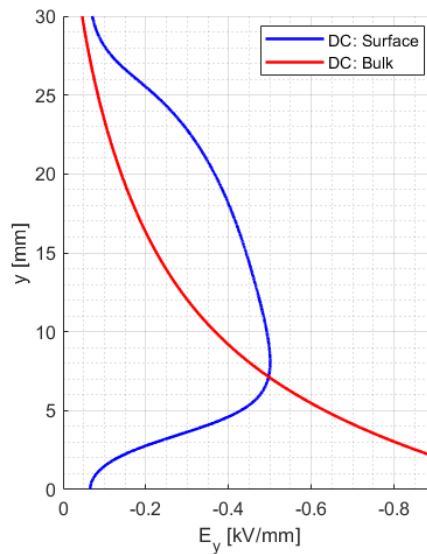


Figure 6.7: Axial steady-state DC field distribution for the surface and the bulk simulated for a temperature gradient of 40 °C and 10 kV electrode voltage

In order to emphasize the contribution of dependence of conductivity on temperature and field (α and β , Table 5.1), the axial steady-state DC bulk field distributions for different α or β values are shown in Figs. 6.8a & 6.8b. Increasing the temperature coefficient α leads to a shift in field towards the colder area, while increasing the field coefficient β leads to a uniform field distributions. However, very high values for β are needed to get significant changes in the field distribution.

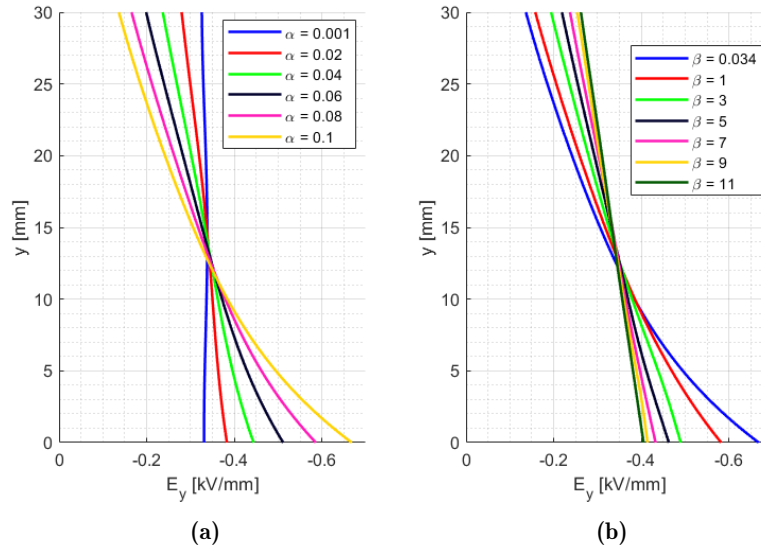


Figure 6.8: Axial steady-state DC field distribution in the bulk with different values for α , 6.8a. Axial steady-state DC field distribution in the bulk with different values for β , 6.8b. For temperature gradient of 20 °C and 10 kV electrode voltage. The y-axis corresponds to the Y-direction of Fig. 5.1.

6.5 Electric field transition with & without thermal gradients

The values of the dielectric time constant τ_d (Eq. 4.15), go from 79 min at 20 °C to 64 min at 40 °C and 27 min at 60 °C, isothermal condition. For temperature gradients the decrease in dielectric time constant is smaller because part of the spacer still has a low conductivity. The effect of the dielectric field constant on the electric field distribution at isothermal 20 °C is displayed in Figs. 6.9a, 6.10a & 6.12a. The setup was energized by a transient with a rising time of 10 s. The results from the previous section are taken for the curves "DC" and "AC (50 Hz)". The remaining curves show profiles corresponding to different values of time, shorter and longer than τ_d . It can be seen that for values of time $\ll \tau_d$ the field is distributed similarly to the sinusoidal AC profile, while for times $\gg \tau_d$ the field distribution tends to match that for steady-state DC. Therefore, the field can still have a sinusoidal AC distribution, although the voltage is already constant for several minutes to hours. Hence, an insulator operating in DC with voltage transients in reality operates in mixed conditions and it must be designed as such. The same behavior can be observed for temperature gradients in Figs. 6.9b, 6.10b & 6.12b. However, the time constant decreased to approx. 75 min (calculated by using the average conductivity for this temperature gradient) instead of 79 min. The field settles therefore just slightly faster than the 20 °C isothermal field, but slower than the 40 °C isothermal field. Since most of the change happens between 0 s and τ_d , the accurate settlement of the field at $5\tau_d$ cannot be observed. The field profiles from the transient simulation fit mostly to the stationary results, except the field profiles in Fig. 6.12b which do not reach the steady-state DC distribution. The reason for that is the high non-linearity of the conductivity together

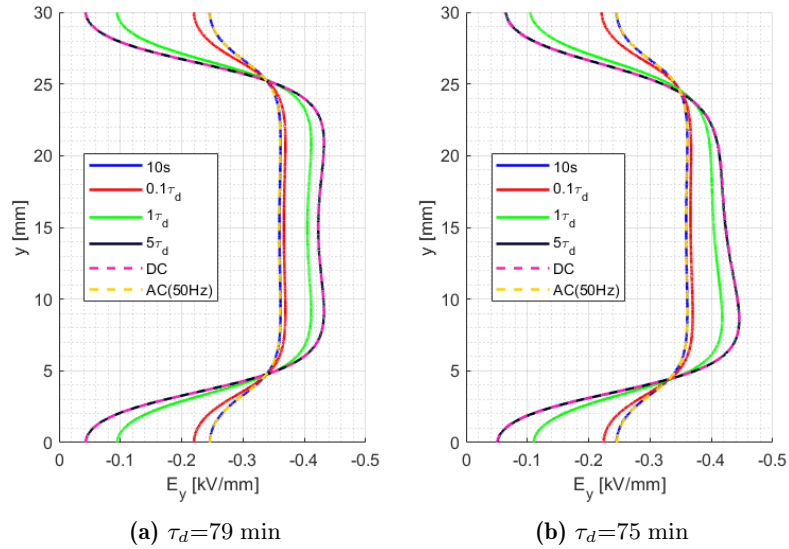


Figure 6.9: Axial the surface field at different points of time after step response, for steady-state DC and sinusoidal AC(50 Hz). Isothermal condition at 20 °C (6.9a) and thermal gradient of 20 °C from top 40 °C to 20 °C at the bottom (6.9b).

with the small distance between high and low temperature, hence COMSOL has difficulties to find an equilibrium in conductivity. Thermal gradients on the spacer increase the surface field in the colder regions, while decreasing it in the hotter regions. An increase in the max. axial surface field of 2 % for a gradient of 20 °C and 15 % for 40 °C was observed. In the bulk, the axial field already increased by 92 % for only a thermal gradient of 20 °C.

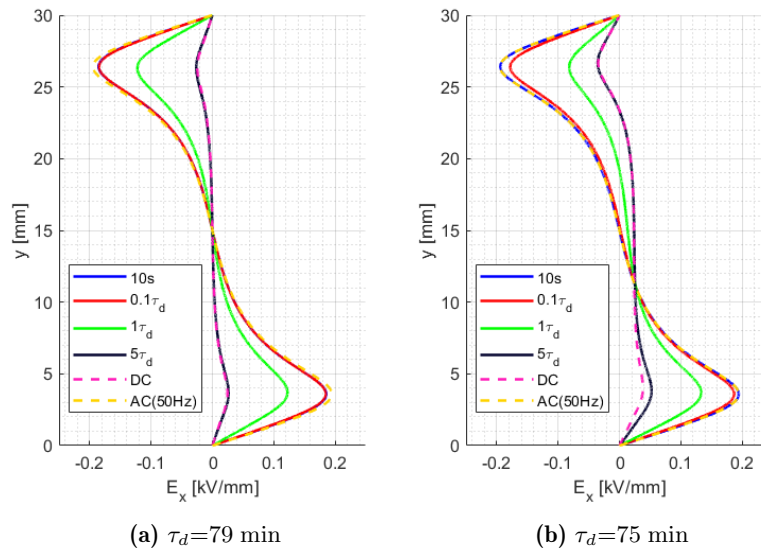


Figure 6.10: Radial surface field at different points of time after step response, for steady-state DC and sinusoidal AC(50 Hz). Isothermal condition at 20 °C (6.10a) and thermal gradient of 20 °C from top 40 °C to 20 °C at the bottom (6.10b).

This puts the spacer under higher stress and can lead to reduction in reliability and life

span, especially for higher thermal gradients, see Fig. 6.11. For the radial field in Fig. 6.10 an opposite change over time is observed as for the axial one. The radial field decreases with time, as is was already mentioned in section 6.4. While the axial field surface or in this case also tangential field is crucial for the generation of PD and therefore more important for field design, the radial field it is important for or normal field in this case plays also a design role, if defects like higher surface roughness, pollution or surface charges are present. Besides the surface field, the field distribution in the bulk is from great interest as well, since the heat distribution and convection can have a stronger impact on the electrical conductivity and therefore yielding higher fields, see Fig. 6.10b.

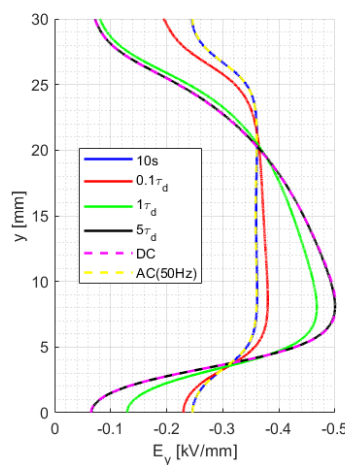


Figure 6.11: Axial surface field at different points of time after step response, for steady-state DC and sinusoidal AC(50 Hz). Time constant $\tau_d=64$ min and thermal gradient of 40 °C from top 60 °C to 20 °C at the bottom.

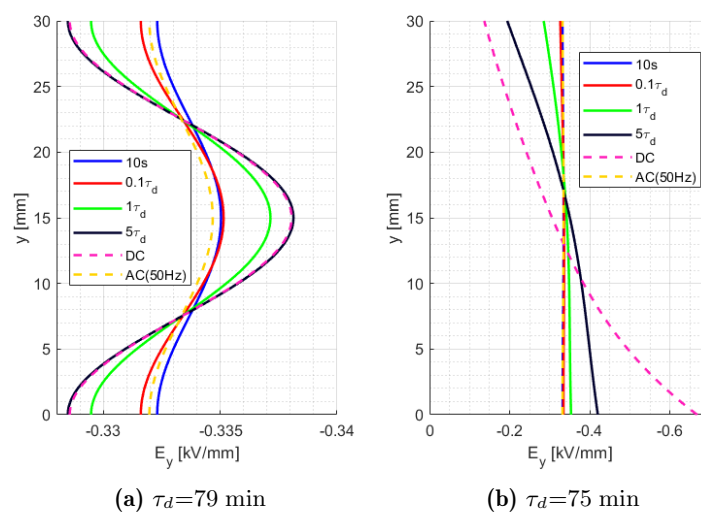


Figure 6.12: Axial bulk field at different points of time after step response, for steady-state DC and sinusoidal AC(50 Hz). Isothermal condition at 20 °C (6.12a) and thermal gradient of 20 °C from top 40 °C to 20 °C at the bottom (6.12b).

6.6 Influence of voltage transients on surface field distribution

Simulations were performed in steady-state DC considering a time that exceeds $5\tau_d$ in an isothermal environment. Three different voltage ramps were applied with rise times of 1 ms, 1 s and 1 min, to reach a steady-state value of 10 kV. After the steady-state voltage was reached, no noticeable difference in field dynamic between the simulations was observed. Indeed τ_d ranges between 79 min at 20 °C and 27 min at 60 °C isothermal conditions, thus times which are orders of magnitude longer than the voltage transient time [12, 13]. In almost every system, especially in power electronics applications, voltage overshoots during switching of solid state components, as well as voltage transients to energize the system and to invert voltage polarity, in addition to load transients, can occur often. These overshoots can reach a voltage peak of 2pu and last up to milliseconds. The maximum and minimum tangential field component for a voltage ramp of 0.1 ms and a voltage step with an overshoot of 2pu with the same duration are reported in Fig. 6.13. The field behaves as the applied voltage and reaches the double of the field strength at the overshoot peak. This fast change is possible because during voltage transients the field is governed by the permittivity. The fast and strong increase in field from the overshoot can lead to partial discharges (PD), which again affect the life span of the insulation component.

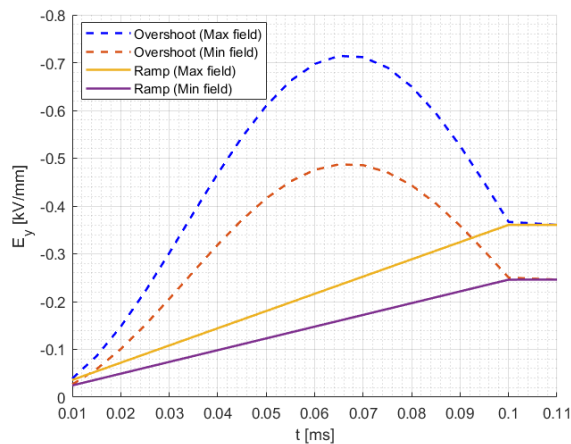


Figure 6.13: Axial surface field over time for different energization slopes. First a voltage step with an overshoot of 2pu and duration of 0.1 ms and second a voltage ramp with a 0.1 ms rising time without overshoot.

Indeed, it has been shown that in high and medium voltage power electronics systems, the high-frequency repetitive impulses whose modulation provides the AC voltage can have significant effect on the life span and reliability of insulation systems, even in the absence of PD. By another example presented in Fig. 6.14, it is shown that the change in voltage (dV/dt) translates directly to the change in field (dE/dt). The maximum axial field is displayed for different slope voltage rising times in Fig. 6.14. First the voltage was increased with a constant slope and rising time 1 s and 0.5 s (blue and red line), and afterwards with an exponentially rising voltage (Eq. 6.1). The field, represented in the figure as the

maximum value, describes a same curve as the applied voltage.

$$v(t) = 10 \text{ kV} \left(1 - e^{-\frac{t}{0.1}}\right) \quad (6.1)$$

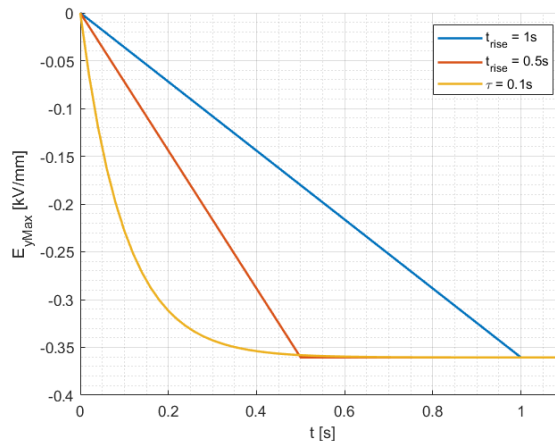


Figure 6.14: Maximum axial surface field over time for different voltage transients. The blue line describes a constant increase with rising time 1 s, red line holds for 0.5 s and the yellow line an exponentially increasing voltage to 10 kV with rising time 0.1 s

6.7 Influence of contamination on surface field distribution

In order to provide a rough, initial approach to contamination effect investigation, the surface layer conductivity was altered to simulate the effect of humidity uniformly distributed on spacer surface. Figure 6.15 reports electric field profiles at the surface layer (interface with air) for steady-state DC, considering the conductivity of air to be $8e-15$ S/m. The axial field profile decreases strongly when the surface conductivity is higher than that of air. For the radial field profiles, the field increases when the surface conductivity deviates from the air conductivity, see curve $8e-14$ and $8e-17$ S/m. For the conductivity value $8e-16$ S/m, the layer smooths the field lines (radial field) transition from air into the bulk. In Fig. 6.16 field profiles of a contaminated surface together with a thermal gradient are presented. It is shown that both field components on the surface strongly change when there are more than one environmental effect present. It is, as well interesting to see, that the conductivity of air plays a major role for the surface field profiles. Different humidity rates in air (tropical areas) will cause an impact on the field value and distribution.

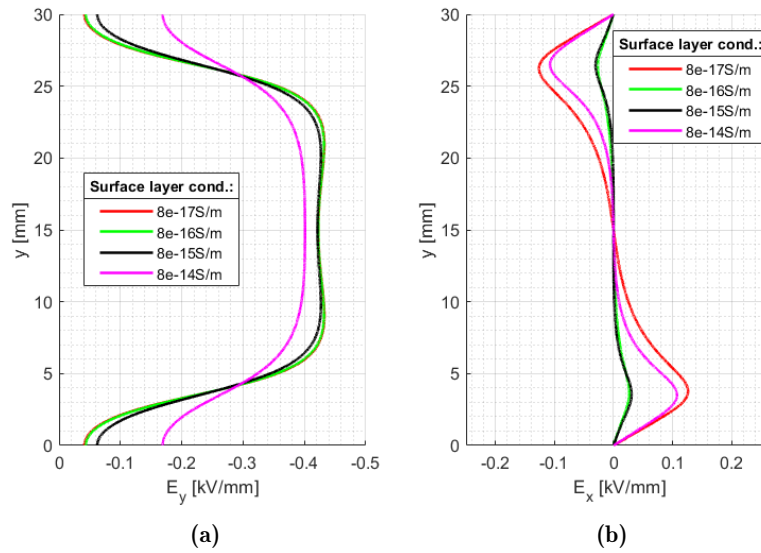


Figure 6.15: Axial (a) and radial (b) surface field for different initial surface conductivity values in steady-state DC. Isothermal condition at 20 °C.

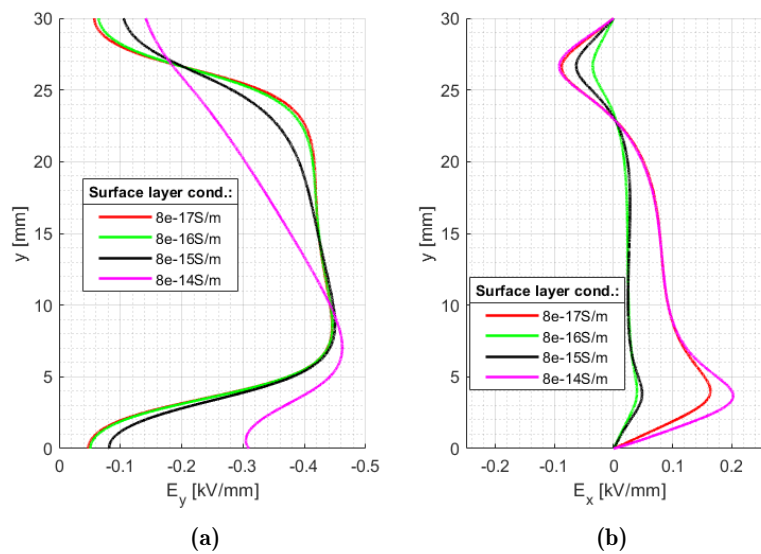


Figure 6.16: Axial (a) and radial (b) surface field for different initial surface conductivity values in steady-state DC. Temperature gradient of 40 °C.

7 Summary/Conclusion

When DC insulation systems are used in an electrical asset where it is known that voltage transients (voltage magnitude variations, energization, polarity inversion, impulses and harmonics) are frequent, they should be designed according to the worst stress conditions provided by AC or DC field distribution, remembering that it is the maximum field that determines life and reliability [14]. It is again the maximum field, which is connected to partial discharge inception [12, 13], and the maximum field can depend in DC on insulation temperature and temperature gradient, thus on load conditions. Therefore, DC insulation system (spacer) design must take various parameters into account, including the insulating material properties, electrothermal and environmental stresses. This may mean that a conservative design, considering the worst conditions, would have to be implemented, as long as the spacer operating conditions expected for all life are not well defined. Concerning the insulating material properties, especially conductivity and its dependence on temperature and electric field, dielectric losses and voltage endurance coefficient have to be known as accurate as possible.

The approach to provide a contribution to face such design issues and complexities has been to implement a simulation model in COMSOL, which combines electro- and thermodynamics and has an electrical conductivity dependent on temperature and electric field. The model was improved step by step, starting only with a stationary simulations for electrostatics and upgrading it by testing and understanding the backgrounds of the software as well as using the theory. The current version of the model is able to simulate stationary and transient processes in AC and DC. With some adjustments the spacer setup can be changed into a bushing or a cable. In order to highlight the relevance of our approach and modelling, this report shows that, at interfaces between bulk and surface, as well as surface and air, the change in conductivity due to temperature gradients can lead to significantly higher field stresses, which can promote surface trees and, in any case, affect spacer reliability. Indeed, even small gradients of 20 °C change the field distribution significantly. Since the field distribution in sinusoidal AC does not vary with temperature gradients, it is straightforward the need to change the design criteria of insulation systems when using them in DC systems. In the presented setup only the axial field shows a significant change, due to the spacers geometry. In more complex geometries, the radial component can as well change significantly. The change in field distribution caused by temperature gradients can lead to faster ageing, inception of partial discharges, etc. as mentioned above, in particular as the field transition from permittivity to conductivity-dependent can take several minutes to hours, thus a non-negligible time during insulation life if the transient rate is (as expected in dynamic, emerging assets) large. Additionally, the transition of the field is faster in warmer areas of the system. In summary, even if design optimization is a challenge, the modelling provided in this work may at least help to avoid to resorting simply to worst conditions and over design a spacer.

To support all the above, experimental validation is planned, using surface potential sensors. A measurement was already carried out, but due to lack of information on the specimen properties it isn't included. Therefore the measurement is going to be repeated in the future when the properties are known. At the very end, the purpose is to provide a viable tool for DC spacer (and later bushing) designers which allow an optimized design, reliable and effective (with the aim to minimize dimensions) to be achieved. Further investigation are also needed in the direction of air conductivity dependence on humidity, surface contamination and the presence of ripple superimposed to the DC voltage. In the future, the current model should be extended with models for surface partial discharges and tracking, to provide useful tools to determine and specify the creepage-based design.

8 List of figures

4.1	Display of an electric field between two opposite charges	10
4.2	Electric field strength vectors at material interface	11
4.3	Orthogonal interface to the el. field in a parallel-plate capacitor	12
4.4	Tangential interface to the el. field in a parallel-plate capacitor	12
5.1	Axis-symmetric drawing of the spacer used for COMSOL simulations with a surface layer of 0.1 mm.	14
5.2	2D axisymmetric model of the setup in COMSOL	15
5.3	Comparison of Eq. 5.6 (full line) and Eq. 5.5 (dotted lines) for different reference temperatures T_0 . The field is 0 kV/mm.	17
5.4	Electric field norm simulated with the “electrostatics“ physic for an electrode voltage of 10 kV DC.	18
5.5	Electric field norm simulated with the “electric currents“ physic	19
5.6	Boundaries fixed to 20 °C.	20
6.1	Changing voltage with isothermal condition (20 °C). Electric field norm (left) and conductivity in the insulator (right). 20 kV (6.1a & 6.1b), 60 kV (6.1c & 6.1d), 100 kV (6.1e & 6.1f)	22
6.2	Constant voltage (0 V) with different temperatures. Temperature (left) and conductivity in the insulator (right). Temperature of the top electrode is 0 °C (6.2a & 6.2b), 20 °C (6.2c & 6.2d), 100 °C (6.2e & 6.2f)	23
6.3	Triangular mesh in the surface layer and surrounding for different surface layer thicknesses. Units in mm.	24
6.4	Steady-state DC field distribution along the surface for different surface layer thicknesses with a thermal gradient of 20 °C between the electrodes. The y-axis corresponds to the Y-direction of Fig. 5.1.	24
6.5	Axial steady-state DC [-] and sinusoidal AC (50 Hz) [-] field distribution for the surface and the bulk, 6.5a. Radial steady-state DC [-] and sinusoidal AC (50 Hz) [-] field distribution for the surface and the bulk, 6.5b. Simulated for isothermal conditions at 20 °C and 10 kV electrode voltage. The y-axis corresponds to the Y-direction of Fig. 5.1.	25
6.6	Axial steady-state DC [-] and sinusoidal AC (50 Hz) [-] field distribution for the surface and the bulk, 6.6a. Radial steady-state DC [-] and sinusoidal AC (50 Hz) [-] field distribution for the surface and the bulk, 6.6b. Tem- perature gradient of 20 °C, nominal voltage 10 kV. The y-axis corresponds to the Y-direction of Fig. 5.1.	26
6.7	Axial steady-state DC field distribution for the surface and the bulk simu- lated for a temperature gradient of 40 °C and 10 kV electrode voltage . . .	26

6.8	Axial steady-state DC field distribution in the bulk with different values for α , 6.8a. Axial steady-state DC field distribution in the bulk with different values for β , 6.8b. For temperature gradient of 20 °C and 10 kV electrode voltage. The y-axis corresponds to the Y-direction of Fig. 5.1.	27
6.9	Axial the surface field at different points of time after step response, for steady-state DC and sinusoidal AC(50 Hz). Isothermal condition at 20 °C (6.9a) and thermal gradient of 20 °C from top 40 °C to 20 °C at the bottom (6.9b).	28
6.10	Radial surface field at different points of time after step response, for steady-state DC and sinusoidal AC(50 Hz). Isothermal condition at 20 °C (6.10a) and thermal gradient of 20 °C from top 40 °C to 20 °C at the bottom (6.10b).	28
6.11	Axial surface field at different points of time after step response, for steady-state DC and sinusoidal AC(50 Hz). Time constant $\tau_d=64$ min and thermal gradient of 40 °C from top 60 °C to 20 °C at the bottom.	29
6.12	Axial bulk field at different points of time after step response, for steady-state DC and sinusoidal AC(50 Hz). Isothermal condition at 20 °C (6.12a) and thermal gradient of 20 °C from top 40 °C to 20 °C at the bottom (6.12b).	29
6.13	Axial surface field over time for different energization slopes. First a voltage step with an overshoot of 2pu and duration of 0.1 ms and second a voltage ramp with a 0.1 ms rising time without overshoot.	30
6.14	Maximum axial surface field over time for different voltage transients. The blue line describes a constant increase with rising time 1 s, red line holds for 0.5 s and the yellow line an exponentially increasing voltage to 10 kV with rising time 0.1 s	31
6.15	Axial (a) and radial (b) surface field for different initial surface conductivity values in steady-state DC. Isothermal condition at 20 °C.	32
6.16	Axial (a) and radial (b) surface field for different initial surface conductivity values in steady-state DC. Temperature gradient of 40 °C.	32

9 List of tables

5.1	Material parameter of the insulator material and air	16
5.2	Constant values used for finding the right reference temperature	17

10 References/Bibliography

- [1] De Doncker, R. W. Power electronic technologies for flexible DC distribution grids. In: *2014 International Power Electronics Conference (IPEC-Hiroshima 2014 - ECCE ASIA)*. 2014, pp. 736–743.
- [2] Olenmark, Andreas, Sloth, Jens, Johnsson, Anna, Wilhelmsson, Carl, and Svensson, Jorgen. Control Development and Modeling for Flexible DC Grids in Modelica. In: 2015, pp. 823–829. Available from DOI: 10.3384/ecp15118823.
- [3] Montanari, G. C. The Potential Impact of Flexible DC Transmission and Distribution on Insulated Cables: Accelerated Aging and Premature Failure. In: *2019 IEEE PES Asia-Pacific Power and Energy Engineering Conference (APPEEC)*. 2019, pp. 1–4.
- [4] Wang, L., Bosworth, M., Hauer, J., Soto, D., Schoder, K., and Steurer, M. Common-Mode Characterization of a Modular Multilevel Converter in a Megawatt-scale Medium-Voltage DC Test Bed. In: *2019 IEEE Electric Ship Technologies Symposium (ESTS)*. 2019, pp. 388–395.
- [5] Montanari, G. C., Hebner, R., Morshuis, P., and Seri, P. An Approach to Insulation Condition Monitoring and Life Assessment in Emerging Electrical Environments. *IEEE Transactions on Power Delivery*. 2019, **34**(4), pp. 1357–1364.
- [6] Montanari, G. C., Seri, P., Franchi Bononi, S., and Albertini, M. Partial discharge behavior and accelerated aging upon repetitive DC cable energization and voltage supply polarity inversion. *IEEE Transactions on Power Delivery*. 2020 (), pp. 1–8.
- [7] Seri, P., Ghosh, R., Cirioni, L., and Montanari, G. C. Partial discharge measurements of DC insulation systems: the influence of the energization transient. In: *2019 IEEE Conference on Electrical Insulation and Dielectric Phenomena (CEIDP)*. 2019, pp. 377–380.
- [8] Kaufhold, M., Aninger, H., Berth, M., Speck, J., and Eberhardt, M. Electrical stress and failure mechanism of the winding insulation in PWM-inverter-fed low-voltage induction motors. *IEEE Transactions on Industrial Electronics*. 2000, **47**(2), pp. 396–402.
- [9] Stone, G., Campbell, S., and Tetreault, S. Inverter-fed drives: which motor stators are at risk? *IEEE Industry Applications Magazine*. 2000, **6**(5), pp. 17–22.
- [10] Seri, P., and Montanari, G. C. A voltage threshold in operating condition of PWM inverters and its impact on reliability of insulation systems in electrified transport applications. *IEEE Transactions on Transportation Electrification*. 2019 (), pp. 1–8.

- [11] KÜchler, A. High Voltage Engineering. 2018 (). ISBN 978-3-642-11993-4. Available from DOI: 10.1007/978-3-642-11993-4.
- [12] Mazzanti, G., and Marzinotto, M. *Extruded cables for high-voltage direct-current transmission: Advances in research and development*. 2013.
- [13] Naderiallaf, H., Seri, P., and Montanari, G. C. Investigating conditions for an unexpected additional source of partial discharges in DC cables: load power variations. *IEEE Trans. on Power Delivery*. 2020 (), pp. 1–8.
- [14] Neumann, C. Dielectric Testing of HVDC gas-insulated systems Fundamentals for a future standard. *CIGRE Convenor of JWG D1/B3.57*. 2020 ().
- [15] Dissado, L.A., and Fothergill, J.C. *Electrical Degradation and Breakdown in Polymers*. London: Peter Peregrinus, 1992.
- [16] Pawar, S., Murugavel, P., and Lal, D. Effect of relative humidity and sea level pressure on electrical conductivity of air over Indian Ocean. *Journal of Geophysical Research*. 2009, 114(). Available from DOI: 10.1029/2007JD009716.
- [17] Occhini, E., and Maschio, G. Electrical characteristics of oil impregnated paper as insulation for HVDC cables. *IEEE Trans. Power Appar. Syst.; (United States)*. 1967, 86(). Available from DOI: 10.1109/TPAS.1967.291959.